Constraining the Surface Flux of Sea Spray Particles from the Southern Ocean

S. Hartery[1], D. Toohey[2], L. Revell[1], K. Sellegri[3], P. Kuma[1], M. Harvey[4], A. J. McDonald[1]

[1]University of Canterbury, Christchurch, New Zealand
[2]University of Colorado Boulder, Boulder, Colorado, USA
[3]Laboratoire de Météorologie Physique (LaMP), CNRS/UCA, Aubière, France
[4]National Institute of Water & Atmospheric Research, Wellington, New Zealand

Key Points:

- Current-era GCMs over-estimate sea spray concentrations relative to measurements in the Ross Sea
- Better constraints for sea spray flux were found by tuning wind-speed based parameterizations to these observations
- Variations in sea surface temperature did not explain further variability within the temperature range studied

Corresponding author: Sean Hartery, `hartery.s.p@gmail.com`

Abstract

Modeling the shortwave radiation balance over the Southern Ocean region remains a challenge for Earth system models. To investigate whether this is related to the representation of aerosol-cloud interactions, we compared measurements of the total number concentration of sea spray generated particles within the Southern Ocean region to model predictions thereof. Measurements were conducted from a container laboratory aboard the R/V *Tangaroa* throughout an austral summer voyage to the Ross Sea. We used source–receptor modeling to calculate the sensitivity of our measurements to upwind surface fluxes. From this approach, we could constrain empirical parameterizations of sea spray surface flux based on surface wind speed and sea surface temperature. A newly tuned parameterization for the flux of sea spray particles based on the near-surface wind speed is presented. Comparisons to existing model parameterizations revealed that present model parameterizations led to over-estimations of sea spray concentrations. In contrast to previous studies, we found that including sea surface temperature as an explanatory variable did not substantially improve model–measurement agreement. To test whether or not the parameterization may be applicable globally, we conducted a similar regression analysis using a database of in situ whitecap measurements. We found that the key fitting parameter within this regression agreed well the parameterization of sea spray flux. Finally, we compared calculations from the best model of surface flux to boundary layer measurements collected onboard an aircraft throughout the Southern Ocean Clouds, Radiation, Aerosol Transport Experimental Study (SOCRATES), finding good agreement overall.

1 Introduction

In the remote boundary layer of the Southern Ocean, continental sources of particulate matter such as black carbon, terrestrial monoterpenes, dusts, and pollen contribute very little to the population of suspended particulate (Murphy et al., 1998). As a result, the magnitudes of the direct and indirect shortwave radiative effects from the suspended particulate within the region are largely driven by local, marine sources (Carslaw et al., 2013; McCoy et al., 2015). There has been a considerable amount of work in recent years to understand the excess of shortwave radiation reaching the ocean surface in the Southern Ocean within climate-chemistry models (CCMs), especially regarding the representation of clouds within these models (Trenberth & Fasullo, 2010; Bodas-Salcedo et al., 2014). Since hygroscopic particulate matter are a necessary precursor to cloud formation, they can indirectly exert a substantial influence on the radiation balance through modification of cloud brightness (Twomey, 1977) and cloud phase through the availability of ice nuclei (DeMott et al., 2010).

The natural sources of airborne particles in the region are the production of sea-spray generated particles (SSPs) from wind–wave interactions and ultra-fine particles from the homogeneous nucleation of sulfuric acid and other volatile vapours. However, the rate of production of SSPs remains an open problem: the number of particles entering the atmosphere of a given droplet size and at a given wind speed has been shown to vary by over an order of magnitude among existing parameterizations for the production of SSPs (Ovadnevaite et al., 2014). If one also accounts for the uncertainties related to predicting the dependence of the surface flux on the wind speed over the water, estimates for the intensity of the surface flux diverge further. As a result, both the concentration and seasonal cycle of SSPs remain poorly constrained in the Southern Ocean (Henzing et al., 2006; Revell et al., 2019). Several studies have shown that the lack of prediction accuracy for the flux of SSPs results in large biases between observed and modelled mass concentrations of SSPs in

the marine boundary layer (MBL), particularly in regions with cold waters (Jaeglé et al., 2011; Grythe et al., 2014; Witek et al., 2016).

In general, sea spray is the dominant source of particulate matter in the Southern Ocean in terms of mass (Murphy et al., 1998); however, during ice formation in coastal Antarctica, wind-blown frost flowers and snow from sea-ice can also become locally prominent sources (Kaleschke et al., 2004; Yang et al., 2008). Since these particles are the largest in the region (Quinn et al., 2017), they are also a substantial contributor to the local aerosol optical depth (AOD) (Shindell et al., 2013). While the contribution of SSPs to the regional AOD is much more significant than its contribution to cloud albedo in the Northern Hemisphere, over the Southern Ocean it is precisely the opposite (Ayash et al., 2008). This highlights that SSPs are a regionally important component of cloud formation over the Southern Ocean. This is not surprising: SSPs are mainly comprised of highly soluble sea salt and so they are very efficient cloud condensation nuclei (CCN) (Petters & Kreidenweis, 2007). While SSPs form only a small fraction of CCN globally, they can make up ∼65% of CCN over the Southern Ocean (Quinn et al., 2017).

Recent studies have also shown that SSPs can act as ice nucleating particles (INPs), which encourage the phase transition of cloud droplets to ice (DeMott et al., 2016; McCluskey et al., 2018). Since the Southern Ocean is far removed from continental sources of INPs (e.g. dust), SSPs may be the only source of INPs in the region. Ice nucleation sites within the droplets are likely a result of suspended amounts of organic material within the sea surface microlayer which became entrained within the droplets during formation (DeMott et al., 2016). However, organic materials form very little of the mass composition of the resulting SSPs (Murphy et al., 1998); hence, the ice-nucleating potential of sea spray is very weak relative to continental sources such as mineral dusts (McCluskey et al., 2018). Still, the capacity for SSPs to modulate cloud phase represents an additional mechanism through which they can affect the local radiation balance.

While we have emphasized the potential radiative effects SSPs might have on the Southern Ocean region, there are other ways in which they can perturb the Earth system. Several studies have shown that the largest SSPs are non-negligible contributors to the exchange of latent and specific heat across the ocean–atmosphere interface (Richter & Sullivan, 2013; Ortiz-Suslow et al., 2016). In a bulk flux model of the air–sea exchange of heat, Andreas et al. (2015) showed that these large, "shear" sea-spray droplets accounted for fluxes of sensible and latent heat on the same order of magnitude as fluxes directly from the ocean–atmosphere interface at high wind speeds ($U_{10} > 15$ m s^{-1}). Observations and model simulations have shown that the rate of momentum transferred from the atmosphere to the ocean starts to decrease after a critical threshold wind speed is passed (30 m s^{-1}; (Powell et al., 2003; Bao et al., 2011; Hwang, 2018)). Theoretical work has suggested that this change is driven by the exchange of sensible heat between the largest droplets and the atmosphere, which become more abundant at high wind speeds (Bao et al., 2011). This leads to considerable biases in the prediction of storm intensity (Bao et al., 2011). The ability to predict the abundance of SSPs is therefore vital to fully understanding many macroscopic processes within the region.

To constrain the potential role sea spray may have on the regional radiation budget, it is first necessary to validate current parameterizations for its flux against in situ observations of its abundance. However, there is currently a dearth of such observations over the Southern Ocean. In this work we present measurements of the total number concentration of airborne particles recorded throughout an austral summer voyage to the Ross Sea aboard the R/V *Tangaroa*. We use these measurements to test existing empirical parameterizations which describe the flux of particles from wave breaking events in open seas. Measurements from instruments

onboard the High-Performance Instrumented Airborne Platform for Environmental Research (HIAPER) throughout the Southern Ocean Clouds, Radiation, Aerosol Transport Experimental Study (SOCRATES) were also used to validate these parameterizations. Since the winds throughout both of these experiments included the extremes of surface conditions encountered at the air–sea interface, understanding the flux of SSPs in this highly dynamic region will be valuable in constraining both current and future flux estimates.

2 Methods

2.1 Measurements

The voyage aboard the R/V *Tangaroa* began on February 9$^{\text{th}}$ and ended on March 21$^{\text{st}}$, 2018 departing and returning to Wellington, New Zealand (41°17' S, 174°46' E). The bulk of the voyage was spent in waters south of 60°S, with 17 days of the voyage spent in seas between 60–70°S and 13 days of the voyage south of 70°S.

In situ measurements of boundary layer aerosol were conducted from a container laboratory on the shelter deck of the R/V *Tangaroa* (2 m a.s.l.). The instruments within the container laboratory drew a continuous air sample through 40 m of 100 mm ID anti-static tubing (EOLU PU; IPL Ltd.) from the mast of the R/V *Tangaroa* (15 m a.s.l.). For the purposes of this study, we have primarily focussed on measurements from the passive cavity aerosol spectrometer probe (PCASP-100X; Droplet Measurement Technologies) with supplementary data from a differential mobility particle sizer (DMPS; TSI). The PCASP-100X is an optical particle counter which measured the number concentration size spectra of particles within the air sample. The instrument is capable of detecting particles with optical diameters between 0.1–3.0 μm in 30 size bins at 1 Hz. The DMPS measured the number concentration size spectra of particles within the air sample with mobility diameters between 0.02–0.3 μm in 32 size bins once every 10 minutes. We have corrected the number concentration measurements according to calculations of the sampling and transport efficiency from Brockman (2001). These calculations accounted for anisokinetic sampling conditions, diffusion of the particles toward the tube walls, and gravitational settling of the particles. All of these calculations were based on empirical parameterizations of these losses in a turbulent flow. Across the spectrum of sizes we measured, we estimate that the total sampling efficiency was at most 93%, but no less than 90%.

Throughout the voyage, a cavity ring-down spectrometer (CRDS; Picarro G2301) measured mole fractions of CO_2, CH_4, and H_2O from a separate sampling line. The sampling line of the CRDS was within 5 m of the main sampling line used for the particulate sampling. Intrusions of ship exhaust from the rear of the ship would have been sufficiently well-mixed in the turbulent air around the ship superstructure so as to affect both sampling lines. We used a threshold limit of 405 ppm of CO_2 to detect when ship exhaust contaminated our main sampling line. This threshold was well above the trend line of the [CO_2] mole fraction time-series. After removing these outliers, we used 1 Hz sub-samples of the particle number concentrations to calculate 1-minute averages of the number concentration size spectra and its standard deviation. When the standard deviation of the 1 Hz samples deviated significantly from Poisson counting statistics the sample was removed.

This study also incorporated measurements from the New Zealand Met Service's Automated Weather Station (AWS) aboard the R/V *Tangaroa*. The AWS anemometer was positioned at 22.5 m a.s.l. on the mast of the ship, while the rest of the AWS was positioned at 15 m a.s.l. The AWS measured: atmospheric pres-

sure, atmospheric temperature, relative humidity, wind speed, wind direction, and accumulated precipitation. Measurements of the average relative wind speed and wind direction were made using a pair of ultrasonic anemometers (Gill WindSonic) and reported at 1-minute intervals. The measurements of wind speed were corrected according to directionally-dependent acceleration factors, based on a model of air flow around the R/V *Tangaroa*'s superstructure (Popinet et al., 2004; Smith et al., 2011). The wind speeds were then corrected according to the ship heading and speed to derive the true wind speed and wind direction. Finally, the acceleration-corrected, true wind speed at 22.5 m was scaled to the 10 m reference level using the bulk flux algorithms developed from the Coupled Ocean-Atmosphere Response Experiment (COARE) (Edson et al., 2013). In employing the COARE bulk flux algorithms, we have not accounted for differences in the height of the AWS due to heave with respect to mean sea level, which may amount to ± 4 m in heavy seas. If for a given measurement, the pitch or roll of the ship was significant with respect to the mean wind vector, then the measured wind speed would have been systematically biased low. However, throughout the voyage, the pitch of the ship was $<20°$, and so these corrections would be less than 6%.

Measurements of the boundary layer number concentration size spectra were also conducted onboard HIAPER, a modified Gulfstream V aircraft, from January 16$^{\text{th}}$–February 24$^{\text{th}}$, 2018. These measurements were part of the SOCRATES experiment. Over the course of the experiment, there were 15 flights, which departed and returned to Hobart, Australia. We have focused on the flights which coincided with our observational record, namely Research Flights (RF) 10–15 which took place between February 7$^{\text{th}}$–24$^{\text{th}}$, 2018. Two Ultra-High Sensitivity Aerosol Spectrometers (UHSAS; Droplet Measurement Technologies) were used throughout the experiment to measure the number concentration size spectra of particles within the surrounding air; however, for this study we focused solely on the measurements from the UHSAS mounted inside of the aircraft. The UHSAS sampled ambient air via a counterflow virtual impactor inlet mounted outside of the aircraft. This ensured that the internal flow rate of the UHSAS was isokinetically matched to the exterior flow around HIAPER. Like the PCASP-100X, the UHSAS is an optical particle counter which can detect particles with optical diameters between 0.059–1.022 μm in 100 discrete size bins at 1 Hz. It was determined that corrections to the number concentration size spectra from the additional ram pressure of sampling the aerosol from a moving aircraft would amount to less than 1%. This was substantially less than the observed variability in both the number concentration time series and the volume flow rate of the pump that provided the flow through the UHSAS. For each flight we identified 3–6 periods when the altitude was stable, there was little precipitation, and the observed number concentration size spectra were relatively stable. In each of these periods, we averaged the number concentration size spectra over 5–10 minutes. This resulted in 28 unique measurements between 69–6,100 m a.s.l, 17 of which were in the boundary layer.

2.2 FLEXPART-WRF

The FLEXible PARTicle transport model (FLEXPART), FLEXPART-WRF, is a Lagrangian particle dispersion model designed to model particle trajectories within mesoscale meteorological fields from the Weather Research & Forecasting Model (WRF) (Brioude et al., 2013). For this study, we used meteorological forecasts from the real-time Antarctic Mesoscale Prediction System (AMPS) (Polar Meteorology Group, Byrd Polar and Climate Research Center, 2018). AMPS uses a variety of data sources to constrain these forecasts, including near-real-time sea-ice concentrations measured from the Special Sensor Microwave/Imager (SSM/I) radiometer and sea surface temperature (SST) data from the National Center for Environmental Prediction (NCEP) (Bromwich et al., 2005). Initial and boundary

conditions for AMPS were specified according to near-real-time forecasts from the NCEP Global Forecasting System (Bromwich et al., 2005). We used the AMPS output with the widest spatial coverage, domain 1, which has a horizontal resolution of 24 × 24 km, a vertical resolution of 61 η levels, and a temporal resolution of three hours. The AMPS forecasts used throughout this study were downloaded from `https://www.earthsystemgrid.org/project/amps.html`.

We initialized 100, 000 particle trajectories from the geographic location of the R/V *Tangaroa* every three hours to match the temporal resolution of AMPS. Additional simulations were run for every hour in between the meteorological time steps if the R/V *Tangaroa* had entered a new grid cell in the AMPS domain. These two criteria resulted in 651 unique simulations. To trace losses due to deposition throughout the simulation, FLEXPART assigned each particle a unit mass distributed over a log-normal size distribution. To match our observations, we centered this distribution around a geometric dry diameter of 0.20 μm ($D_{p,g}$ = 0.4 μm at 80% relative humidity), with a geometric standard deviation of 2.00, and a dry density of 1.84 g cm^{-3}. FLEXPART-WRF used the discretized Langevin equation to describe the turbulent dispersion of these particles through the atmosphere in reverse time with an adaptive time-step strictly less than 180 s. The particles were advected through the meteorological fields specified by AMPS from the time of measurement up to five days prior in reverse time. Throughout the trajectory, losses of particle mass due to dry deposition were calculated according to the resistance method (Hicks et al., 1987). To improve these calculations we modified FLEXPART-WRF to account for hygroscopic particle growth according to the ambient relative humidity (Gerber, 1985), since changes in particle size can significantly affect a particle's settling velocity and dry deposition velocity. FLEXPART-WRF also accounted for losses of particle mass from precipitation and droplet activation. Within clouds, FLEXPART-WRF calculated the scavenging rate of particles from droplet activation according to the parameterization of Hertel et al. (1995). For scavenging by precipitation below cloud, loss rates were estimated from the following empirical relationship:

$$\Lambda = A I_s^B \tag{1}$$

where the scavenging rate, Λ, was calculated as a function of the rain-equivalent snow intensity, I_s (mm hr^{-1}), and user-set scavenging coefficients, A and B. While fairly good representations of particle scavenging from rain exist in the literature, there is substantially more uncertainty with regards to the scavenging from snow (Slinn, 1977). Recent parameterizations of below-cloud scavenging in the non-WRF version of FLEXPART recommend applying an empirical fit to a set of snow scavenging rates measured in southern Finland (Kyrö et al., 2009; Grythe et al., 2017). However, this parameterization doesn't explicitly account for increases in scavenging with increasing snow intensity. We observed that the differences in scavenging rates Kyrö et al. (2009) observed across the particle size spectra were small compared to the difference in median snow scavenging rates they observed between their median observed snow intensity (0.2 mm hr^{-1}) and peak snow intensity (5 mm hr^{-1}). We used the median scavenging rates and snow intensity values they reported to estimate the following scavenging coefficients for snow: A = 4×10^{-5} and B = 0.43. For reference, the typical values used by FLEXPART-WRF for rain are 5×10^{-6} and 0.62, respectively. Together with the dry deposition velocity, the mass concentration loss rate could be described at any point in the simulation by the following:

$$\frac{\mathrm{d}m}{\mathrm{d}t} = -\left(\frac{v_d}{h} + \Lambda\right) m \tag{2}$$

where m is the mass of the particle, v_d is the dry deposition velocity, and h was the height of the layer in which dry deposition occurred (30 m a.s.l.).

In reverse mode, FLEXPART-WRF calculated the residence time of the particles within the lowest 100 m of the atmosphere. The residence time calculation was weighted by the local air density and the residual mass of the particles within the grid-cell. The weighted residence time was normalized by the initial mass of the particles such that the resulting residence time accounted for losses from wet and dry deposition as described above. Finally, FLEXPART-WRF integrated the weighted residence time over the duration of the meteorological time-step for each grid-cell of the AMPS domain.

2.3 Quantifying the contribution of sea spray

Previous studies have shown that in pristine marine environments, the contribution of SSPs to the number concentration size spectra can be characterized by a single log-normal number concentration size distribution (Modini et al., 2015; Quinn et al., 2017). Distributions derived from this method have been shown to agree well with number concentration size spectra measured during laboratory wave-breaking experiments and the "canonical sea spray size distribution" derived from other studies (Prather et al., 2013; Lewis & Schwartz, 2004). This also agrees with the mass composition of the particles measured in the Southern Ocean boundary layer during the ACE-1 campaign, which found that particles larger than 0.3 μm were composed almost entirely of sea-salt (Murphy et al., 1998). We applied this methodology to our own measurements of the number concentration size spectra from the PCASP-100X; i.e. we fit a number concentration size spectra, $\mathrm{d}n(\mathrm{d}\log D_p)^{-1}$, of the following form:

$$\frac{\mathrm{d}n}{\mathrm{d}\log D_p} = \frac{N}{\sqrt{2\pi}\log(\sigma_g)} \exp\left[-\frac{\log^2\left(\frac{D_p}{D_{p,g}}\right)}{2\log^2(\sigma_g)}\right] \tag{3}$$

where D_p is the particle diameter, N is the total number concentration of particles, $D_{p,g}$ is the geometric mean diameter of the distribution, and σ_g is the geometric standard deviation of the distribution. After fitting, the retrieved spectra were corrected to a relative humidity of 80% (Gerber, 1985). In the process of fitting, the geometric standard deviation (σ_g) of the mode was fixed to a value of 2, which best fit our data. While Modini et al. (2015) and Quinn et al. (2017) allowed σ_g to freely vary in their regression analysis, the variance-covariance matrix from our regression indicated that the resulting parameters were significantly correlated, since the data very weakly constrained σ_g.

To calculate the total number concentration of sea spray from the FLEXPART-WRF residence time, we assumed that the surface flux of SSPs also followed a log-normal distribution:

$$\frac{\partial f}{\partial \log D_p} = \frac{F}{\sqrt{2\pi}\log(\sigma_g)} \exp\left[-\frac{\log^2\left(\frac{D_p}{D_{p,g}}\right)}{2\log^2(\sigma_g)}\right] \tag{4}$$

where f is the partial particle flux in $\mathrm{m}^{-2}\ \mathrm{s}^{-1}$, F is the total particle flux in $\mathrm{m}^{-2}\ \mathrm{s}^{-1}$, and D_p is the particle diameter.

The most widely used empirical approach for constraining the particle flux from the ocean surface is the "whitecap method". It results from the following assumptions: first, that the total flux of particles entering the atmosphere from the ocean surface can be determined from the fractional surface coverage of whitecaps, W ("whitecap fraction"); second, that the whitecap fraction can be adequately determined from the 10 m scalar wind speed over the ocean, U_{10}; and third, that the shape of the SSP size distribution is not a function of wind speed. Laboratory and field experiments have shown that all of these assumptions are reasonable (Monahan

& Ó Muircheartaigh, 1980; Monahan et al., 1986). Hence, the total number of particles entering the atmosphere, F, can be predicted from just the 10 m wind speed, U_{10}:

$$F = \frac{E}{\tau} W(U_{10}) \qquad F = \alpha W(U_{10}) \tag{5}$$

where W is a function that models how the surface coverage of whitecaps increases as a function of wind speed, E is the number of particles produced per whitecap, and τ is the lifetime of the whitecaps. Since we can only hope to constrain one constant pre-factor, we combine both E and τ into a single parameter α, which we assume to be constant. Historically, the whitecap function W has been assumed to be a simple power-law, based on early field observations of whitecap formation (Monahan, 1971). However, it has since been well-established that whitecaps do not form in the open ocean until the 10 m wind speed exceeds 3–4 m s^{-1}, which is a feature that cannot be described by a power-law model (A. Callaghan et al., 2008; Schwendeman & Thomson, 2015; Bell et al., 2017). We considered three other wind-dependent models of the surface flux that incorporated a threshold wind speed below which very few SSPs are produced:

$$\begin{aligned} W_{PL} &= a_1 {U_{10}}^{a_2} \\ W_C(U_{10}) &= \begin{cases} b_1 \left(U_{10} - b_2\right)^3, & U_{10} \geq b_2 \\ 0, & U_{10} < b_2 \end{cases} \\ W_F(U_{10}) &= 1 - \Phi\left(\frac{c_1}{\sqrt{U_{10}}}\right) \\ W_{LLPL}(U_{10}) &= \frac{d_1 {U_{10}}^{d_2}}{1 + \left(\frac{U_{10}}{d_3}\right)^{-d_4}} \end{aligned} \tag{6}$$

where a_x, b_x, c_x and d_x and are empirical parameters determined from regression analysis with our observations, and Φ is the error function. The first function, W_{PL} ('PL' = 'Power-Law'), is as previously introduced. The second function, W_C ('C' = 'Cubic'), has been used to match more recent field observations of whitecaps (A. Callaghan et al., 2008; Schwendeman & Thomson, 2015)). The third function, W_F ('F' = 'Fetch'), was based on the theoretical work of Snyder and Kennedy (1983), who developed a model of whitecap production based on a fetch dependent threshold for wave breaking. While the work of Xu et al. (2000) showed that the whitecap fraction could be fully determined from the model of Snyder and Kennedy (1983) if both the wind speed and fetch were known, the fetch was typically unlimited throughout our observation period. In high fetch regimes, the coverage of whitecaps is only very weakly dependent on variations in fetch (Piazzola et al., 2002). As a result, we treated c_1, which is a function of the fetch, as a free parameter to be determined through regression, since a single value should accurately describe the data. The last function, W_{LLPL} ('LLPL' = 'Log-Logistic Power-Law') combined the power-law with a log-logistic curve to emulate the threshold mechanism. While W_{PL}, W_C and W_{LLPL} predict that the surface flux will continue increasing as a function of wind speed, the Fetch model (W_F) is the only model which predicts that there exists an upper bound on the particle flux at high wind speeds.

There has also been some debate as to how the temperature of the sea water might moderate whitecap formation (Mårtensson et al., 2003; Sellegri et al., 2006; Jaeglé et al., 2011; Zábori et al., 2012; A. H. Callaghan et al., 2014; Grythe et al., 2014). This was tested directly with SST data from NCEP, which was available from the AMPS forecasts. Thus, the model of surface flux was expanded to:

$$\begin{aligned} F &= \alpha(T_w) W(U_{10}) \\ \alpha(T_w) &= \alpha_0 (1 + \alpha_1 T_w) \end{aligned} \tag{7}$$

where the coefficient α, which describes both the lifetime of the whitecaps and the number of particles produced per whitecap, is now a function of the SST, T_w. Note that, in reality, parameters α_0 and other scaling coefficients within W (e.g. a_1, b_1, d_1) cannot be determined independently, so they are combined into a single parameter for each regression (e.g. $a_1^* = a_1\alpha$). Finally, we assumed that the surface flux was well-mixed within the lowest atmospheric grid cell in FLEXPART-WRF, h = 100 m. Following these assumptions, the number concentration of particles in the SSP mode, $\hat{N}$, was calculated according to:

$$\hat{N}_i = \frac{1}{h} \int_{-t_0}^{0} \iint_{O} F(1 - C_{ice}) \, \mathrm{d}\mathcal{P}_i \tag{8}$$

where t_0 was the length of the FLEXPART-WRF simulation, C_{ice} was the fractional surface coverage of sea ice, O denotes that the integral was only integrated over oceans, and $\mathcal{P}_i$ was the map of footprint residence times for the observation i.

A non-linear least-squares regression analysis optimized the set of parameters for each surface flux model, W, being tested. Parameter optimization was achieved with the Gauss-Newton algorithm, where the goodness-of-fit was measured by the Nash-Sutcliffe model efficiency coefficient (NSE):

$$NSE = 1 - \frac{\sum_{i=1}^{m} \left(N_i - \hat{N}_i\right)^2}{\sum_{i=1}^{m} \left(N_i - \overline{N}\right)^2} \tag{9}$$

where m was the total number of observations and $\overline{N}$ represents the average of every measurement of N_i within the dataset (Nash & Sutcliffe, 1970). To account for differences between the number of parameters between models, we also calculated the Akaike Information Criterion (AIC), which penalized models with more parameters (Akaike, 1974):

$$AIC = 2k + m \log\left(\frac{1}{m} \sum_{i=1}^{m} \left(N_i - \hat{N}_i\right)^2\right) \tag{10}$$

where k was the total number of parameters for a given model. The best model of surface flux was the model which minimized the AIC.

3 Results

3.1 Comparisons Between Surface Meteorological Measurements and Model Forecasts

To demonstrate that the transport simulations produced a meaningful link between the observations and surface fluxes, it was necessary to first validate the Antarctic Mesoscale Prediction System's meteorological fields against the record of observations from the Automated Weather Station (AWS) aboard the R/V *Tangaroa*. As described in the Section 2.1, the AWS measured wind speeds at 22.5 m, which were corrected to the 10 m reference height according to the COARE 3.5 bulk flux algorithms. The corrected wind speeds were compared to the 10 m wind speeds predicted by the AMPS forecasts by matching the location of the R/V *Tangaroa* to the nearest grid-cell within AMPS. This comparison is presented in Fig. 1. The correlation coefficients calculated for both the wind speed (R = 0.81) and wind direction ($R_\circ$ = 0.78) between observations and forecasts were both significant ($p<0.01$), where $R_\circ$ represents the circular correlation coefficient (Fisher & Lee, 1986).

Despite the good agreement we found between the measured and forecast winds, there was no spatio-temporal correlation between the rain-equivalent snow

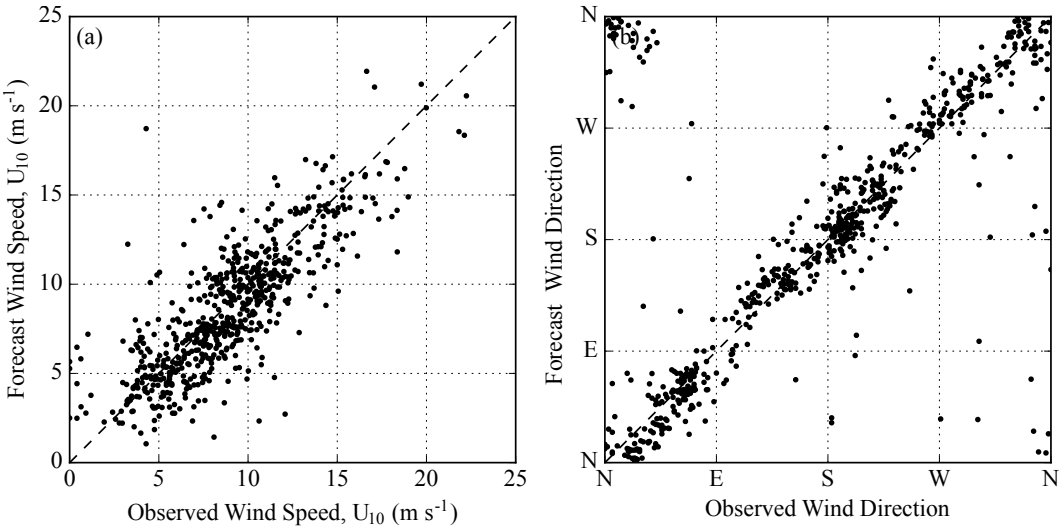

Figure 1. (a) The hourly 10 m scalar wind speeds from the AMPS forecasts were compared to the corrected wind speed (see Section 2.1) observed on the R/V *Tangaroa*. (b) The hourly 10 m wind direction.

rate measured aboard the R/V *Tangaroa* and the precipitation fields forecast by AMPS. However, the climatological distribution of the rain-equivalent snow rate was at least consistent between measurements and forecasts. This suggests that even if precipitation was not spatially consistent with our observations, it was at least as frequent, and of the right intensity within the AMPS forecasts. While comparing localized, discrete events like precipitation can be challenging, even comparing our measurements to grid cells within 100 km and within 6 hours of the R/V *Tangaroa* measurements did not produce a significant correlation.

3.2 Source–Receptor Modeling

In Fig. 2a we show the cumulative five-day, near-surface, residence time for all of the source–receptor simulations described in Section 2.2. The track of the R/V *Tangaroa* throughout the voyage has also been shown for reference. As expected, the near-surface residence time was greatest near the R/V *Tangaroa*. This indicated that our measurements were most sensitive to surface fluxes near the ship. To understand how dry deposition might govern the concentration of SSPs, we also ran several FLEXPART-WRF simulations in which the dry deposition velocity was set to a fixed rate. However, the consistent turbulence of the atmosphere over the Southern Ocean meant that the simulated particles were often very evenly dispersed throughout the boundary layer. As a result, dry deposition was severely limited throughout all of the simulations. Predicted surface flux sensitivities within these simulations only began to diverge after 1–2 days had elapsed in simulation time; however, by then the residence time was typically less than 5% of what it was near the ship. Hence, dry deposition was not a strong factor controlling the concentration of SSPs.

It was evident from Fig. 2a, however, that our observations near the Ross Ice shelf were sensitive to non-marine sources. The fraction of the time the particles spent above non-marine surfaces throughout their five-day simulations increased rapidly as the R/V *Tangaroa* approached Cape Adare, Antarctica. Throughout this period we observed strong, southerly winds, which brought continental, Antarctic air

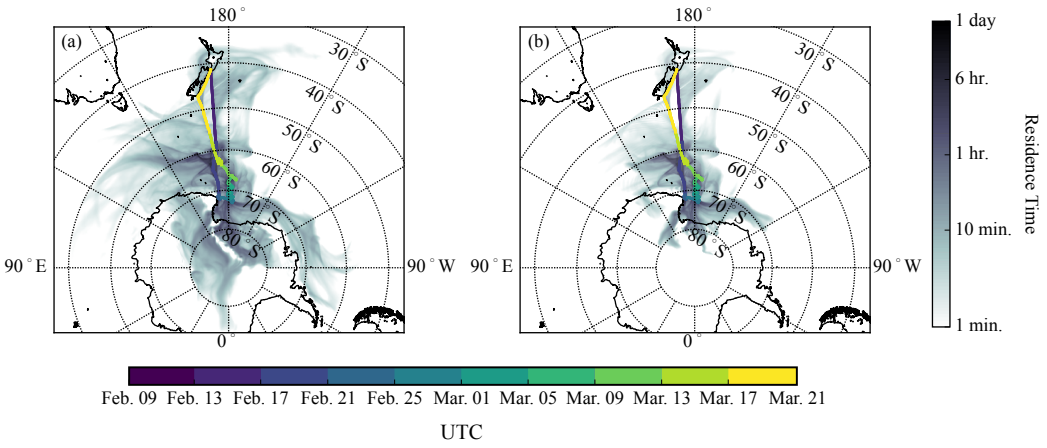

Figure 2. (a) A map of the cumulative near-surface residence time derived from FLEXPART-WRF particle dispersion simulations. The model simulated the transport of $1{\times}10^5$ 0.2 μm particles in reverse time from the time of measurement to five days prior. The near-surface residence time is simply the total amount of time the particle spent below 100 m a.g.l. Within FLEXPART-WRF the transport of the particles was calculated according to meteorological forecasts from the Antarctic Mesoscale Prediction System (AMPS). (b) The same map, but now for a 48-hr. simulation. The colored line in both panels marks the track of the R/V *Tangaroa* throughout the voyage.

across the Ross Ice Shelf. Intrusions of continental air into the MBL are a common phenomenon within the region (Coggins et al., 2014; Coggins & McDonald, 2015). Near the end of the observation period, after March 18$^{\text{th}}$, 2018, the source–receptor simulations showed that our measurements were also sensitive to surface fluxes from the South Island of New Zealand. This was a direct result of the strong northerlies we observed throughout our return transect.

As we identified in Section 3.1, the rain-equivalent snow rates forecast by AMPS were not well-correlated with snowfall intensity measured onboard the R/V *Tangaroa*. While the frequency of occurrence of these events seemed consistent, it is important to note that the wet deposition scheme used by FLEXPART-WRF implicitly assumed that in-cloud activation events only occurred within a precipitating cloud. Hence, the frequency of in-cloud scavenging events was almost certainly under-estimated within the source–receptor simulations. As Hertel et al. (1995) note, the magnitude of the loss of particles to in-cloud activation is almost always greater than either below-cloud scavenging or dry deposition. In fact, an activation event is always strong enough to terminate a particle trajectory within FLEXPART-WRF. Therefore, it was expected that the source–receptor modeling vastly over-estimated the near surface residence time by continuing to advect particles that should have been completely scavenged by cloud. However, a lack of boundary layer cloud within the simulation did not stem from this issue alone. It has been well-established that there is currently a large shortwave radiation bias over the Southern Ocean (Bodas-Salcedo et al., 2014). Observations of cloud base height from radiosondes and ceilometer measurements throughout this same voyage showed that the shortwave radiation bias is related to the lack of low-level cloud and fog predicted within atmospheric models (Kuma et al., 2019). Therefore, it is reasonable to expect that even with an improved in-cloud activation scheme (e.g. Grythe et al. (2017)), FLEXPART-WRF still would have under-estimated the frequency

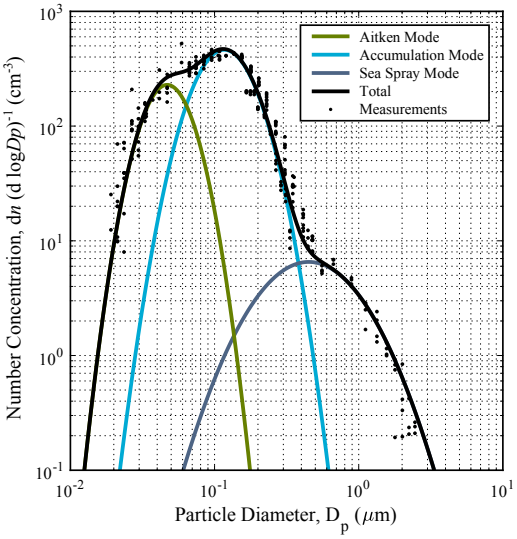

Figure 3. Number concentration size spectra measured from the PCASP-100X (0.1–3μm) and the DMPS (0.02–0.3μm) on February 20$^{\text{th}}$, 2018 at 1300 UTC. Particle sizes have been corrected to 80% relative humidity (Gerber, 1985). Number concentrations for particles larger than 0.5 μm were used to constrain a single log-normal number concentration size distribution ("SSP mode"). This method has been used by other researchers (e.g. Modini et al. (2015) and Quinn et al. (2017)) to constrain the contribution of SSPs to the total number concentration size spectra. The Aitken and accumulation modes are shown for reference.

of droplet activation events. This would have a substantial impact on our source–receptor calculations, resulting in significantly less ocean surface area contributing to the integral in Eq. (8). To visualize this effect, we have also shown the cumulative near surface residence time for a two-day simulation in Fig. 2b, instead of the five-day simulation shown in Fig. 2a. This is addressed further in Section 3.4.

3.3 Number Concentrations of Sea Spray

In Fig. 3 we show an example modal analysis of a number concentration size spectrum measured by the PCASP-100X and DMPS aboard the R/V *Tangaroa*. The size spectra were used to constrain three log-normal "modes" which represented the entire size distribution. The largest of these modes, the SSP mode, is so-named as it has been shown to be comprised almost solely of SSPs (Modini et al., 2015; Quinn et al., 2017). At each hour of observation throughout the voyage we constrained the SSP mode from the spectral measurements shown in Fig. 3, resulting in the time series of the total number concentration of SSPs shown in Fig. 4. In general it was sufficient to constrain the SSP mode from just the PCASP-100X measurements, so the measurements from the DMPS were not used in this study, but are shown for reference. Throughout the entire voyage, we observed the median and standard deviation of the geometric mean diameter of the SSP mode to be 0.4 $\pm$ 0.05 μm at a relative humidity of 80%. This agreed well with the observations of Quinn et al. (2017) in the Southern Ocean. This also agreed with the median dry diameter of SSPs measured from laboratory generated waves, 140–200 nm (Prather et al., 2013), since SSPs are twice as large at 80% relative humidity compared to dry conditions (Gerber, 1985).

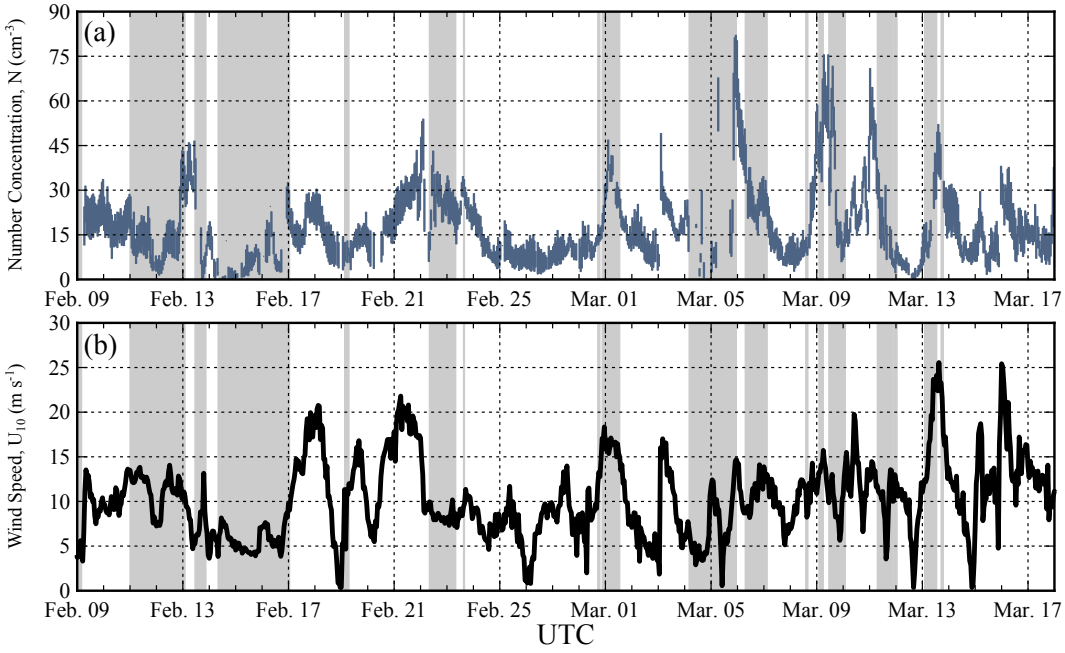

Figure 4. (a) The average hourly number concentration of sea spray particles is shown for the entire campaign with periods of fog (RH>98%) or rain (>1 mm hr^{-1}) marked by the shaded areas. (b) The hourly 10 m wind speed.

In Fig. 4a, the total number concentrations of SSPs and the 10 m scalar wind speeds measured are shown from the beginning of the voyage, February 9$^{\text{th}}$, 2018, until March 18$^{\text{th}}$, 2018. Throughout the voyage, there were several periods when either fog or precipitation was observed at the ship. As expected, fog very efficiently scavenged the particles in the SSP mode through droplet activation processes, much more so than precipitation. However, the lack of observed particles during such events meant that the SSP mode could not be constrained. This is particularly evident around March 5$^{\text{th}}$, 2018. In the last three days of the voyage, March 18$^{\text{th}}$–21$^{\text{st}}$, 2018, we encountered strong northerly winds along the coast of New Zealand, which transported terrestrial particles to the R/V *Tangaroa*. The addition of these non-SSPs resulted in number concentration size spectra from which the SSP mode could not be constrained. As a result, measurements when fog or precipitation was observed at the ship, or when there was a significant influence from New Zealand were excluded from the regression analysis presented in the following section.

In Fig. 4b we also show the 10 m wind speed throughout the same period of measurement. We observed that when winds were light ($U_{10} < 4$ m s^{-1}) the total number concentration of particles in the SSP mode was no more than 10 cm^{-3}, and had a median of 7 cm^{-3}. Light-wind periods (U_{10}<4 m s^{-1}) occurred 14% of the time in upwind conditions, as weighted by the near surface residence time. However, during a light-wind period on March 12$^{\text{th}}$, 2018, there appeared to be no particles at all. This agreed well with the transport modeling in Fig. 2, which showed that during all light-wind periods, except the period occurring on March 12$^{\text{th}}$, the particles had a significant near surface residence time over Antarctica. While the boundary layer over Antarctica is generally a very pristine environment, human activity from research stations near the Ross Ice shelf and exposed mountain faces both represent potential sources for the concentration of particles observed at low wind speeds. In the regression analysis that followed, the median concentration of SSPs observed at

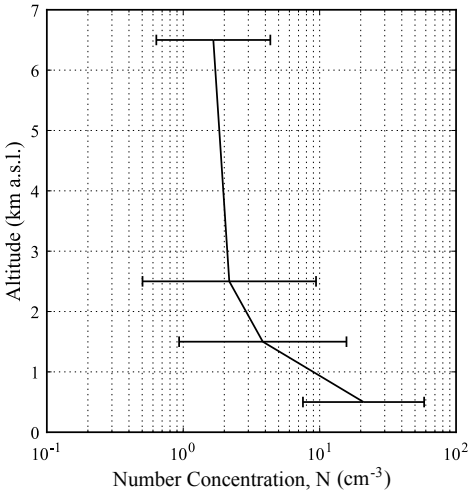

Figure 5. The total number concentration of sea spray generated particles is shown as a function of altitude over the course of several flights aboard HIAPER, (RF 11–15). The ranges within each altitude bin show the minimum and maximum number concentration observed. Flights RF 11–15 took place on the following days, in order: Feb. 17$^{\text{th}}$, 18$^{\text{th}}$, 20$^{\text{th}}$, 21$^{\text{st}}$ and 24$^{\text{th}}$, 2018.

low wind speeds was removed from the observations (except for the period around March 12$^{\text{th}}$, 2018). After removing this background concentration, we calculated the hourly-averaged number concentration of particles in the SSP mode to be 9 cm^{-3}, with a maximum of 62 cm^{-3}.

In Fig. 5 we show the total number concentration of SSPs derived from the UHSAS number concentration size spectra onboard HIAPER. These measurements were taken over the course of several flights in February 2018 to illustrate the range of concentrations observed within each 1 km bin. The measurements within one kilometer of the Earth's surface were always determined to be below-cloud (if any cloud was present) and within the boundary layer. In contrast, all other bins were determined to be above cloud (if any cloud was present) and above the boundary layer. From Fig. 5 we can also identify that there was always at least 5–10 cm^{-3} of SSPs in the boundary layer, which is consistent with the measurements at low wind speeds on board the R/V *Tangaroa*. As expected, there were also very few SSPs above the cloud, indicating that nearly all of these particles had been consumed during cloud formation.

3.4 Regression Analysis

Predicted SSP concentrations can be obtained by integrating Eq. (8); however, we have already identified that particle losses from in-cloud scavenging represented the greatest uncertainty to our source–receptor modeling. To address this within the regression analysis we allowed the simulation length, t_0, to vary as a free parameter within Eq. (8). In effect, this allowed the regression to estimate the return rate of a droplet activation event within a boundary layer cloud (e.g. fog or marine stratocumulus) or a significant precipitation event (>10 mm hr^{-1}). Either of these events would have efficiently scavenged the particle, thereby terminating its trajectory. This approach is similar to the Statistical Wet Deposition method used by other researchers, which prescribes the length of time it takes a surface flux of

particles to fully mix into the boundary layer after a precipitation event or cyclone (e.g. Ovadnevaite et al. (2014)).

Table 1. The values listed in this table are the relative likelihood that a given parameterization of surface flux correctly predicted the observed number concentration of sea spray generated particles relative to the best parameterization. These values were calculated from the difference between the Aikake Information Criterion (AIC) of each parameterization and the AIC of the best parameterization (AIC_b) according to the following: $\exp(-0.5(AIC - AIC_b))$ (Burnham & Anderson, 2002). The AIC measures the log-likelihood that a given surface flux parameterization minimizes the residual sum of squares between predicted and observed concentrations while also penalizing parameterizations which include large numbers of parameters (Akaike, 1974). See Eq (6) for parameterization definitions.

Surface Flux parameterization	W_{PL} ‡	W_C †	W_F §	W_{LLPL} ††
$F(U_{10})$	$<1\times10^{-3}$	$<1\times10^{-3}$	1	0.2
$F(U_{10}, T_w)$	$<1\times10^{-3}$	$<1\times10^{-3}$	0.6	$<1\times10^{-3}$

‡Power-Law; †Cubic; §Fetch; ††Log-Logistic Power-Law.

In Table 1 we have calculated the relative likelihood that a given surface flux parameterization fit the data as compared to the best parameterization, W_F. We used the relative probabilities in Table 1 to compare two parameterizations: for instance, modelling the flux with W_F and a function of sea surface temperature was only 60% as likely to optimally fit our data as using W_F alone. We also found that regardless of the surface flux parameterization, the optimal simulation length, t_0 was 48 ± 3 hours. This is similar to the "filling time" Ovadnevaite et al. (2014) used to characterize surface fluxes of SSPs from their measurements in the North Atlantic. The filling time is a characteristic timescale used in the Statistical Wet Deposition Method for determining sea spray fluxes from a concentration time series (Lewis & Schwartz, 2004). Definition of the filling time varies by author. In Ovadnevaite et al. (2014), they interpret the filling time as "...the time between the cyclone formation and subsequent arrival to [the measurement location]" instead of "the time since the last precipitation event as considered in (Lewis & Schwartz, 2004)". The filling time we determined is consistent with the average time that elapsed between the passage of seven separate cyclones we encountered throughout March, 2018. These cyclones provided widespread high winds and boundary layer cloud, resulting in high fluxes, but relatively short lifetimes for any suspended particulate. Hence, our finding is consistent with the definition of filling time given by Ovadnevaite et al. (2014).

According to the AIC, the best parameterization for the surface flux of SSPs, F, used the fetch parameterization for whitecaps, W_F (Snyder & Kennedy, 1983; Xu et al., 2000):

$$\begin{aligned} \frac{\partial f}{\partial \log D_p} &= \frac{F}{\sqrt{2\pi}\log(2)} \exp\left[-\frac{\log^2\left(\frac{D_p}{0.4}\right)}{2\log^2(2)}\right] \\ F &= \alpha W_F(U_{10}) \\ \alpha &= 3.6\times10^7 \\ W_F(U_{10}) &= 1 - \Phi\left(\frac{6.5}{\sqrt{U_{10}}}\right) \end{aligned} \tag{11}$$

where D_p is the particle diameter in μm at a relative humidity of 80%.

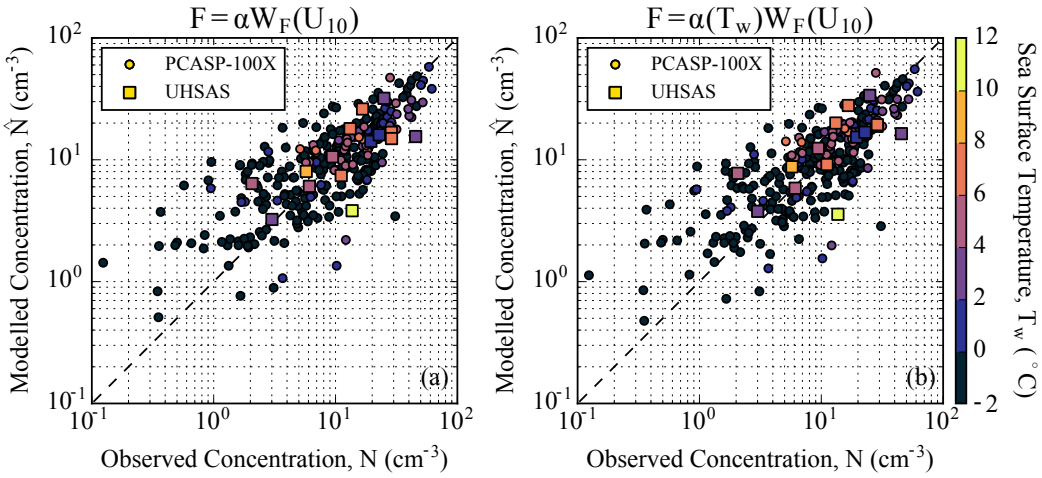

Figure 6. **(a)** Predicted concentrations of sea spray generated particles from the best parameterization of surface flux are compared to measurements from two observation platforms: a PCASP-100X aboard the R/V *Tangaroa* and the UHSAS onboard HIAPER. The best parameterization for the surface flux, F, of these particles was a function of the wind speed over the ocean surface. Each model–measurement pair is colored according to the average SST, weighted by the near-surface residence time. **(b)** As in (a), but for a parameterization of surface flux which incorporated a linear function of SST in addition to the wind speed dependence.

In Fig. 6a we show the model–measurement residuals for the best parameterization of surface flux. The model–measurement residuals have been color-coded according to the average SST. The average values of SST were weighted by the two-day, near-surface residence time. On average, the predicted concentrations did not appear to be biased positive or negative. However, a recent study by Jaeglé et al. (2011) showed that particle fluxes may significantly depend on SST. Changes in SST result in changes to the water viscosity. This is thought to modify the length of time for the whitecap to dissipate, τ, which is part of the constant, α. Hence, in order to compare to their result, we fit a linear correction term for the constant α presented in Eq. (11) as a function of the SST, T_w, finding:

$$\alpha(T_w) \;=\; 3.6 \times 10^7 (1 + 0.024 T_w) \tag{12}$$

The model–measurement residuals of the temperature-corrected parameterization, are shown in Fig. 6b. From Table 1 we can see that this did not substantially improve model fidelity. In both Figs. 6a and b we have also shown the model–measurement pairs for the SOCRATES observations within the boundary layer. Since these measurements were not included within the regression framework, the good agreement in both of these figures provides a measure of confidence that Eq. (11) produces reasonable results within the Southern Ocean region.

In Fig. 7a we show the predicted flux of SSPs from each of the models in Eq. (6) as a function of near-surface wind speed. The total particle flux predicted by Gong (2003) has also been shown for reference. In Fig. 7b we have compared the linear function of SST we recovered from the regression analysis to the polynomial function fit by Jaeglé et al. (2011). We have shifted the values of the polynomial function so that it matches our linear function at T_w = -2°C. The slope of our linear function predicts that SST is not as significant a control of SSP surface flux as shown by Jaeglé et al. (2011). This may be a result of the distribution of our mea-

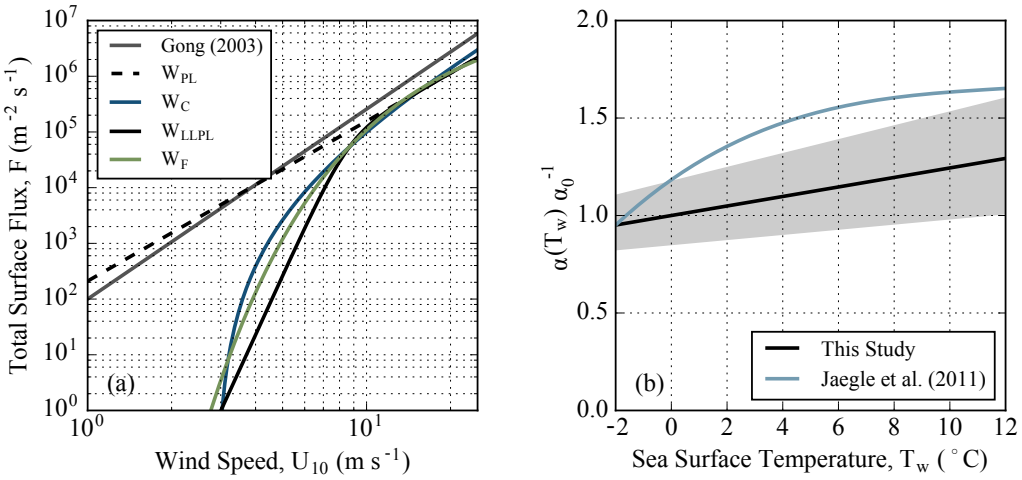

Figure 7. (a) The best parameterization of the total surface flux of sea spray generated particles, W_F, is compared to calculations from the Gong (2003) parameterization. (b) The linear bias correction function found by the regression is compared to the function reported by Jaeglé et al. (2011), where their function has been shifted vertically to match the linear bias correction function at T = -2° C. The shaded region shows how uncertainty in the retrieved regression parameters propagated to prediction uncertainty.

surements across different SST regimes since 78% of our observations were related to waters in a narrow temperature range (-2–0°C). Hence, there would be little improvement to either the NSE or AIC for these samples. Still, as shown in Fig. 7b, the bias correction curve presented by Jaeglé et al. (2011) is clearly outside of the uncertainty bounds for the modest temperature dependence we observe within our dataset.

Finally, we compared the Nash-Sutcliffe model efficiency coefficient (NSE) for the best parameterization we found within our regression framework to two different parameterizations of SSP surface flux. The NSE is generally equivalent to R^2, but can also become negative when the average observed concentration provides a better fit to the data than the proposed parameterization. From Table 2 it is clear that Eq. (11) predicted concentrations of SSPs that were more consistent with our observations than predictions from either the Gong (2003) or the Jaeglé et al. (2011) parameterizations. Comparisons showed that the Gong (2003) parameterization produced too many SSPs at all wind speeds.

For reference, we also performed the regression for the entire five-day simulation. In all of the parameterizations presented, the NSE decreased significantly for the longer simulation, consistent with our hypothesis that in-cloud droplet activation was not accurately simulated. In addition, surface fluxes predicted by W_F when constrained by the five-day simulations were strictly smaller than surface fluxes predicted by W_F when constrained by the two-day simulations, for all wind speeds. Therefore, our finding that the parameterization of Gong (2003) over-predicted the surface flux of SSPs was robust.

3.5 Meta-Analysis of Whitecap Data

In order to assess the conditions under which the parameterization presented above may be applicable, we analyzed global whitecap data from the literature. In

Table 2. The Nash-Sutcliffe model efficiency coefficient between the number concentration of SSPs predicted by a given surface flux parameterization and the observation conducted aboard the R/V *Tangaroa*. The time, t_0, is the length of time for which the Lagrangian particle dispersion parameterization simulated the movement of SSPs back in time. A negative value for the NSE implied that the mean of the observations was better at predicting the observed variance than the given parameterization, whereas a value of 1 would imply a perfect model–measurement fit.

Surface Flux parameterization	NSE (t_0 = 48 hours)	NSE (t_0 = 120 hours)
(Gong, 2003)	<0	<0
(Jaeglé et al., 2011)	0.22	<0
Eq. (11)	0.67	0.52

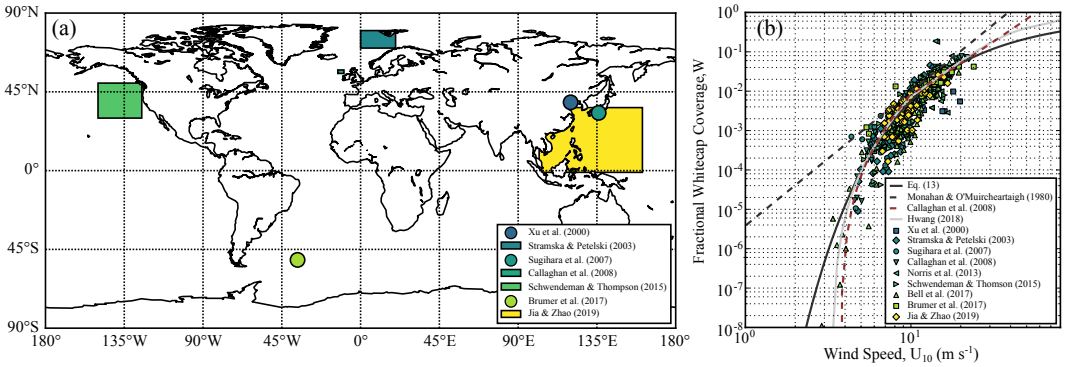

Figure 8. (a) The spatial extent of shipborne and tower whitecap observations within the database assembled for the whitecap meta-analysis. Studies where the coordinates of the observations were not specified all took place in the North Atlantic. (b) The fractional coverage of the sea surface by whitecaps as a function of 10 m wind speed.

Fig. 8b we have amalgamated 527 in situ ship-borne and tower observations of the surface coverage of whitecaps as a function of the 10 m wind speed, U_{10} (Xu et al., 2000; Stramska & Petelski, 2003; Sugihara et al., 2007; A. Callaghan et al., 2008; Norris et al., 2013; Schwendeman & Thomson, 2015; Bell et al., 2017; Brumer et al., 2017; Jia & Zhao, 2019). Studies published after the year 2000 were used since they all employed some form of automated image processing. This meant that each whitecap measurement was a result of $>10^2$ images, a necessary minimum to have a convergent mean (A. H. Callaghan & White, 2009). The spatial coverage of these studies is shown in Fig. 8a, indicating that there is a good degree of coverage across surface temperature regimes within the database. In Fig. 8b we have shown three parameterizations for the whitecap coverage from the literature overlying the in situ measurements (Monahan & Ó Muircheartaigh, 1980; A. Callaghan et al., 2008; Hwang, 2018). We used the AIC to compare the existing parameterizations shown in Fig. 8b to the fetch model, which was fit to the data via non-linear least-squares regression. We found that the fetch model for whitecap development captured the variability in the database best, with the relative likelihood that the other models accurately captured the variability being $<10^{-3}$. It also did so with a continuous function, whereas the other models were piece-wise. The best fit for the whitecap data was as follows:

$$W_F = 1 - \Phi\left(\frac{6.2}{\sqrt{U_{10}}}\right) \tag{13}$$

We also sought to validate the dependence of SSP fluxes on SST. However, SST data within the works cited were either not included or simply summarized as a range of values encountered. Still, most voyages made their measurements within a fairly narrow SST band. Hence, we could test whether or not there was any dependence by using a voyage-average SST for each study. Using the AIC as a measure of the goodness of fit, we found that SST did not improve the regression. This is evident by visually comparing the observations of Jia and Zhao (2019), which took place in extremely warm seas (T_w ~28°C), to the rest of the data points.

4 Discussion

4.1 Meteorological Measurements

In the previous section, we presented total number concentrations of SSPs within the Southern Ocean marine boundary layer as measured from two separate measurement platforms. These were compared to estimations of the total number concentration of SSPs derived from a source–receptor analysis. To assess the validity of the meteorological fields used within the source–receptor analysis, we compared the near-surface winds forecast by AMPS to our observations aboard the R/V *Tangaroa*. We found that the near-surface winds forecast by AMPS compared favorably to our observed winds with respect to both magnitude and direction. Previous studies have found large biases between AMPS forecasts and the true, local winds over the complex coastal topography of the Antarctic coastline (Bromwich et al., 2005; Jolly et al., 2016). However, ocean waves have much less surface roughness in comparison to the coastal topography of Antarctica, which would suggest that this may not be as substantial an issue over the ocean.

While the precipitation fields forecast by AMPS did not correlate well with our measurements, the climatological distribution of precipitation events within AMPS was consistent with our observations. However, within FLEXPART-WRF a lack of precipitation "trickled up" to the cloud layer: in the current version of FLEXPART-WRF, clouds are only present within a simulation if they are precipitating. As a result, scavenging of SSPs from in-cloud activation was likely poorly modeled within the AMPS–FLEXPART-WRF framework. As our own observational record showed, SSPs were strongly scavenged by boundary layer cloud (e.g. fog), particularly through February 15–17$^{\text{th}}$ and March 4–6$^{\text{th}}$, 2018. It is useful, however, to recall that clouds over the Southern Ocean are not very well represented within modern atmospheric models (Trenberth & Fasullo, 2010; Schuddeboom et al., 2019). Current era atmospheric models systematically under-predict the amount of low-lying cloud and fog relative to the true cloud observed over the Southern Ocean (Kuma et al., 2019). Hence, even if a state-of-the-art microphysical parameterization of in-cloud scavenging had been present in FLEXPART-WRF, it is likely that the scavenging of sea spray still would have been under-estimated.

4.2 Source–Receptor Modelling

Once we had established that there was a missing sink of sea spray within our source–receptor framework, it was necessary to decouple this sink from each of the parameterizations of surface flux we tested within the regression analysis. This was accomplished by allowing the simulation length to vary as a free parameter within the regression analysis. The simulation length can be interpreted as the average length of time since a boundary layer in-cloud activation event (e.g. fog or low-cloud). From Table 2 it is evident that our observations were better reproduced for a fixed simulation length of two days, rather than the five days originally simulated. This agreed well with the "filling time" of 1.5–2 days used by Ovadnevaite et al. (2014) to constrain the surface flux of sea spray in the North Atlantic. While setting

a voyage-wide simulation time may have been a gross approximation, it was likely the only approach in light of the present systematic cloud biases over the Southern Ocean.

4.3 Regression Analysis

By constraining the missing sink of sea spray within our model framework, we could finally compare how well the near-surface wind speed and SST predicted our observational record. We found that the fetch parameterization presented by Xu et al. (2000) and Snyder and Kennedy (1983) performed the best in our comparison as measured by the Nash-Sutcliffe model efficiency coefficient, NSE, and the Akaike Information Criterion, AIC. The parameterization, W_F, is so-named since the parameter c_1 is a function of the fetch. In our analysis we have assumed that this parameter was constant, since fetch does not significantly influence the degree of whitecapping in open seas (Hsu, 1986; Piazzola et al., 2002). Later, when we performed a similar regression analysis with a database of whitecap coverage observations, we found a slightly smaller value for c_1. When we compared Eq. (11) to Eq. (13), we found that c_1 retrieved from the whitecap regression was 6.2 ± 0.2, which was consistent with the value of 6.5 ± 0.2 we retrieved from the SSP regression. The sensitivity of W_F means that Eq. (11) will under-estimate whitecap coverage globally and subsequently result in under-estimations of sea spray fluxes. However, we can compare to the value for c_1 retrieved when we only consider Southern Ocean whitecap data from Brumer et al. (2017) ($c_1 = 6.4 \pm 0.1$). Combined with the goodness of fit to the SOCRATES data (Fig. 7a), this provides a secondary measure of validation for the parameterization over the Southern Ocean. We can only conclude that for a global study, a value for c_1 of 6.2 may be more appropriate. For Southern Ocean specific studies a value for c_1 of 6.5 should be used.

Finally, we compared results from two other parameterizations for the surface flux of SSPs to our observations. We found that neither the Jaeglé et al. (2011) nor the Gong (2003) parameterization could predict the concentration of SSPs we observed over the Southern Ocean as well as Eq. (11). This is connected to how the Gong (2003) parameterization (which Jaeglé et al. (2011) re-scaled) scales the surface flux of SSPs with increasing wind speed. Within this parameterization, the scaling is estimated via a power-law relationship between the surface coverage of whitecaps and near-surface wind speed (Monahan & Ó Muircheartaigh, 1980). However, as we show in Fig. 8b, the parameterization presented by Monahan and Ó Muircheartaigh (1980) results in consistent over-estimations of the whitecap coverage. These over-estimations propagate through the SSP flux parameterization of Gong (2003) and lead to the over-estimations in concentrations we observe. In addition, the power-law predicts that there will always be a flux of sea spray from the ocean surface, despite it being well-established that whitecaps do not form until the wind speed over the ocean exceeds 3–4 m s^{-1}. Even the re-scaled Gong (2003) parameterization presented in Jaeglé et al. (2011) did not match our observations well, either.

4.4 The Effect of Sea Surface Temperature

To understand differences between whitecapping in different regions, previous research has focused on wave parameters and SST. As Sugihara et al. (2007) and Goddijn-Murphy et al. (2011) have shown, there is a marked difference between observations of whitecaps in a pure windsea vs. a swell dominated sea. Indeed, when we fit W_F to the whitecap data from Sugihara et al. (2007) we retrieved a value for c_1 of 6.1 ± 0.1 in a pure windsea (indicating higher spatial coverage of whitecapping) compared to 6.7 ± 0.1 when the winds were following swell or counter swell (indicating lower spatial coverage of whitecapping). This could potentially

explain the difference between the value of c_1 we retrieved from our measurements and the one retrieved from the entire whitecap database. However, conversely, in a satellite-derived whitecap database, Albert et al. (2016) found that whitecaps were not dependent on wave parameters, but were actually modestly dependent on SST. They noted that the lack of dependence on wave parameters may have been a result of using wind history as a proxy for wave age and spatial averaging. However, we found that there was no dependence on SST within the database of in situ whitecap observations.

Of course, even if SST does not affect the fractional coverage of whitecaps, it can still affect the surface flux of particles through changes to viscosity. Results from laboratory studies are mixed: while two studies have clearly shown that the surface flux of sea spray should increase in warmer waters (Mårtensson et al., 2003; Sellegri et al., 2006), others found that that differences in seawater composition (A. H. Callaghan et al., 2014) and wave characteristics (A. H. Callaghan et al., 2012) could be much more important. Other laboratory results have even shown that increases in water temperature led to decreases in sea spray fluxes (Zábori et al., 2012). To test whether or not changes in SST affected our own observations, we used SST as a second independent variable within the regression analysis. We found that the impact to the model–measurement fit was more modest than predicted by Jaeglé et al. (2011) (see Fig. 7b), and that the parameterization which only used wind speed (Eq. (11)) performed just as well. As we noted, this may have been a result of making observations in a very narrow range of SSTs, which would result in very small changes to the regression metrics we analyzed. However, from Fig. 6b we can see that the model–measurement residuals don't appear to be significantly biased from the 1:1 line at warm temperatures.

Ultimately, we should be cautious when implementing temperature correction functions for SSP fluxes. Consider that field observations have already clearly shown that the presence of swell inhibits the surface fraction of whitecaps for a given wind speed (Sugihara et al., 2007). Hence, global climatologies of swell could potentially explain the latitudinal trends in SSP flux expected by (Jaeglé et al., 2011): swell rarely occurs in the tropics (where fluxes are expected to be higher), whereas swell frequently is present at high latitudes (where fluxes are expected to be lower) (Jiang & Chen, 2013). As a result, the resulting bias correction curve Jaeglé et al. (2011) derived from in situ and satellite observations of aerosol may be partially dependent on the presence (or absence) of swell. Yet, the curve attributed the latitudinal variations in flux necessary to fit their observations completely to variations in SST. Our own observations, which were made exclusively in the presence of swell, showed that the dependence of SSP fluxes on SST was much weaker than anticipated by Jaeglé et al. (2011), leading to a very negligible effect on model performance. We conclude that a more comprehensive global study of sea spray which fully controls for upwind wave and SST conditions is needed in order to decouple these two effects. In the interim, models should be cautious in implementing functions which could potentially over-exaggerate radiative feedback loops.

4.5 The Direct Radiative Effect

As the goal of this study was to understand how SSPs might influence the local radiation budget, it would be useful to evaluate whether or not changes to the parameterization of SSP fluxes result in substantial changes within existing climate-chemistry models (CCMs). A recent study comparing the winter-time AOD over the Southern Ocean found that current era parameterizations (e.g. Gong (2003)) of sea spray within a climate-chemistry model (CCM) resulted in over-estimations of the AOD relative to satellite observations (Revell et al., 2019). However, in the austral summer, the opposite was observed: namely, a lack of particles formed from

the nucleation of sulfate-gasses resulted in under-estimates of AOD. Within this same study, the parameterization of surface flux, W_{PL}, was implemented within the CCM to better constrain the contribution of SSPs to the total particle population (Revell et al., 2019). While W_{PL} was not the best function determined by this work, it was similar in form to the Gong (2003) currently implemented within the CCM being studied, so it was an easy substitution. Since W_{PL} had a Nash-Sutcliffe coefficient of 0.6 it also produced results that were consistent with Eq. (11). It is important to note that W_{PL} was used to re-scale the size distribution of the Gong (2003) parameterization, so any changes would be related to differences in the scaling function and not to differences between size distributions. Results conclusively showed that the more conservative estimates of the surface flux of SSPs generated by W_{PL} completely removed the bias in winter-time AOD that was previously observed. Therefore, we are confident that the parameterization for the surface flux of SSPs presented in Eq. (11) will result in better predictions of the abundance of SSPs within the Southern Ocean region. More importantly, Revell et al. (2019) show that it helps disentangle the potential compensating errors in predicting the AOD for studies interested in the more complicated gas phase and aqueous phase chemistry which produces sulfate particles from volatile marine precursors like dimethylsulfide.

As we have emphasized throughout this study, the MBL over the Southern Ocean region is home to the strongest surface winds over open ocean on Earth (I. Young, 1999). Surface winds also appear to be getting stronger: at Macquarie Island, winds have increased in intensity by 3 cm s^{-1} per year from 1973–2011, with satellite data showing that winds over the Ross Sea increased by 0.5–1% through 1991–2008 (Hande et al., 2012; I. R. Young et al., 2011). Within the Ross Sea region, this increase is related to the deepening of the Amundsen Sea low, an area of climatologically low pressure in the Southern Ocean which influences regional winds, sea-ice extent and temperature (Coggins & McDonald, 2015; Raphael et al., 2016). As we show throughout this study, sea spray has a highly non-linear relationship with wind speed. Given their large contribution to the CCN population (10–65%; Quinn et al. (2017)), AOD (Murphy et al., 1998; Revell et al., 2019), and cloud phase (McCluskey et al., 2018) over the Southern Ocean, these particles can have a significant buffering effect on the local climate. We would therefore encourage future studies interested in climate projections for the Southern Ocean to make use of Eq. (11) when predicting the surface flux of sea spray generated particles.

5 Conclusions

In this study, we described and optimized an existing parameterization for the surface flux of sea spray generated particles (SSPs) based on the 10 m wind speed in Eq. (11). Within our regression framework we found that the dependence of SSP fluxes on SST was very weak in the temperature range of our observations ($T_w < 12$ °C) and that it did not help to constrain additional variability in our data set. An external database of previously published whitecap observations was exploited to test the parameterization we used in this analysis and found no temperature dependence at all. While others have shown that temperature-dependent flux parameterizations seem to explain known latitudinal variations in SSP flux, the correction functions derived from such an analysis could potentially be a proxy for latitudinal variations in wave characteristics. Given the potential links between SSPs and the Southern Ocean radiation budget, we should be cautious to add feedback loops where none may exist.

Finally, the parameterization presented in this study is already being used to model the AOD and concentration of CCN in the region. Research has shown that the new parameterization vastly improved regional calculations of AOD, compared with previous parameterizations which over-predicted the surface flux of

SSPs (Revell et al., 2019). We recommend that studies interested in aerosol–cloud interactions implement the parameterization as it has been shown to better constrain the contribution of SSPs to the CCN population.

Acknowledgments

This project was funded through the New Zealand Deep South National Science Challenge Cloud and Aerosols project (2017–19). The Antarctic voyage operations were supported through a New Zealand Crown Funding Agreement and associated voyage science was funded through the National Institute of Water and Atmospheric Research's Research Programme in Ocean-Climate Interactions (2017/19 SCI). SOCRATES measurements were supported by award number AGS-1660537 from the U.S. National Science Foundation. S.P.H. acknowledges support from the University of Canterbury Doctoral Scholarship. D.W.T. acknowledges support from the University of Canterbury Erskine Programme during a 2018 sabbatical to collaborate on this project. L.E.R. was supported by the Deep South National Science Challenge (grant C01X1412) and acknowledges China Southern for partial support. K.S. has received funding from the European Research Council (ERC) under the European Union's Horizon 2020 research and innovation programme (Sea2Cloud grant agreement No 771369) for contributing to this work. The authors would like to acknowledge R/V *Tangaroa* Captain Evan Solly, fellow officers and associated crew for safe passage throughout the voyage in addition to the fellow sea-going scientific staff and voyage leader Dr David Bowden. Thanks especially to those talented and capable crew of the R/V *Tangaroa* who installed both the temporary air inlet and the container laboratory in which this study was conducted. Additional thanks are owed to John McGregor and Gordon Brailsford for underway Picarro CO_2 measurements and to Nick Eton for his help troubleshooting technical issues throughout the voyage.

References

Akaike, H. (1974). A new look at the statistical model identification. *IEEE Transactions on Automatic Control*, *19*(6), 716-723. doi: 10.1109/TAC.1974.1100705

Albert, M. F. M. A., Anguelova, M. D., Manders, A. M. M., Schaap, M., & de Leeuw, G. (2016). Parameterization of oceanic whitecap fraction based on satellite observations. *Atmospheric Chemistry and Physics*, *16*(21), 13725–13751. doi: 10.5194/acp-16-13725-2016

Andreas, E. L., Mahrt, L., & Vickers, D. (2015). An improved bulk air–sea surface flux algorithm, including spray-mediated transfer. *Quarterly Journal of the Royal Meteorological Society*, *141*(687), 642-654. doi: 10.1002/qj.2424

Ayash, T., Gong, S., & Jia, C. Q. (2008). Direct and indirect shortwave radiative effects of sea salt aerosols. *Journal of Climate*, *21*(13), 3207-3220. doi: 10.1175/2007JCLI2063.1

Bao, J.-W., Fairall, C. W., Michelson, S. A., & Bianco, L. (2011). Parameterizations of sea-spray impact on the air–sea momentum and heat fluxes. *Monthly Weather Review*, *139*(12), 3781-3797. doi: 10.1175/MWR-D-11-00007.1

Bell, T. G., Landwehr, S., Miller, S. D., de Bruyn, W. J., Callaghan, A. H., Scanlon, B., … Saltzman, E. S. (2017). Estimation of bubble-mediated air–sea gas exchange from concurrent DMS and CO_2 transfer velocities at intermediate–high wind speeds. *Atmospheric Chemistry and Physics*, *17*(14), 9019–9033. doi: 10.5194/acp-17-9019-2017

Bodas-Salcedo, A., Williams, K. D., Ringer, M. A., Beau, I., Cole, J. N., Dufresne, J.-L., … Yokohata, T. (2014). Origins of the solar radiation biases over the Southern Ocean in CFMIP2 models. *Journal of Climate*, *27*(1), 41–56.

Brioude, J., Arnold, D., Stohl, A., Cassiani, M., Morton, D., Seibert, P., … Wotawa,

G. (2013). The Lagrangian particle dispersion model FLEXPART-WRF version 3.1. *Geoscientific Model Development*, *6*(6), 1889–1904. doi: 10.5194/gmd-6-1889-2013

Brockman, J. (2001). Sampling and transport of aerosols. In P. A. Baron & K. Willeke (Eds.), *Aerosol measurement: Principles, techniques, and applications* (2nd ed., pp. 143–197). Hoboken, NJ: John Wiley and Sons, Inc.

Bromwich, D. H., Monaghan, A. J., Manning, K. W., & Powers, J. G. (2005). Real-time forecasting for the Antarctic: An evaluation of the Antarctic Mesoscale Prediction System (AMPS). *Monthly Weather Review*, *133*(3), 579–603. doi: 10.1175/MWR-2881.1

Brumer, S. E., Zappa, C. J., Brooks, I. M., Tamura, H., Brown, S. M., Blomquist, B. W., … Cifuentes-Lorenzen, A. (2017). Whitecap coverage dependence on wind and wave statistics as observed during so gasex and hiwings. *Journal of Physical Oceanography*, *47*(9), 2211-2235. doi: 10.1175/JPO-D-17-0005.1

Burnham, K. P., & Anderson, D. R. (2002). *Model selection and multimodel inference* (2nd ed.). Springer-Verlag New York. doi: 10.1007/b97636

Callaghan, A., de Leeuw, G., Cohen, L., & O'Dowd, C. D. (2008). Relationship of oceanic whitecap coverage to wind speed and wind history. *Geophysical Research Letters*, *35*(23). doi: 10.1029/2008GL036165

Callaghan, A. H., Deane, G. B., Stokes, M. D., & Ward, B. (2012). Observed variation in the decay time of oceanic whitecap foam. *Journal of Geophysical Research: Oceans*, *117*(C9). doi: 10.1029/2012JC008147

Callaghan, A. H., Stokes, M. D., & Deane, G. B. (2014). The effect of water temperature on air entrainment, bubble plumes, and surface foam in a laboratory breaking-wave analog. *Journal of Geophysical Research: Oceans*, *119*(11), 7463-7482. doi: 10.1002/2014JC010351

Callaghan, A. H., & White, M. (2009). Automated processing of sea surface images for the determination of whitecap coverage. *Journal of Atmospheric and Oceanic Technology*, *26*(2), 383-394. doi: 10.1175/2008JTECHO634.1

Carslaw, K. S., Lee, L. A., Reddington, C. L., Pringle, K. J., Rap, A., Forster, P. M., … Pierce, J. R. (2013). Large contribution of natural aerosols to uncertainty in indirect forcing. *Nature*, *503*, 67-71. doi: 10.1038/nature12674

Coggins, J. H. J., & McDonald, A. J. (2015). The influence of the Amundsen Sea low on the winds in the Ross Sea and surroundings: Insights from a synoptic climatology. *Journal of Geophysical Research: Atmospheres*, *120*(6), 2167-2189. doi: 10.1002/2014JD022830

Coggins, J. H. J., McDonald, A. J., & Jolly, B. (2014). Synoptic climatology of the Ross Ice Shelf and Ross Sea region of Antarctica: k-means clustering and validation. *International Journal of Climatology*, *34*(7), 2330-2348. doi: 10.1002/joc.3842

DeMott, P. J., Hill, T. C. J., McCluskey, C. S., Prather, K. A., Collins, D. B., Sullivan, R. C., … Franc, G. D. (2016). Sea spray aerosol as a unique source of ice nucleating particles. *Proceedings of the National Academy of Sciences*, *113*(21), 5797–5803. doi: 10.1073/pnas.1514034112

DeMott, P. J., Prenni, A. J., Liu, X., Kreidenweis, S. M., Petters, M. D., Twohy, C. H., … Rogers, D. C. (2010). Predicting global atmospheric ice nuclei distributions and their impacts on climate. *Proceedings of the National Academy of Sciences*, *107*(25), 11217–11222. doi: 10.1073/pnas.0910818107

Edson, J. B., Jampana, V., Weller, R. A., Bigorre, S. P., Plueddemann, A. J., Fairall, C. W., … Hersbach, H. (2013). On the exchange of momentum over the open ocean. *Journal of Physical Oceanography*, *43*(8), 1589–1610. doi: 10.1175/JPO-D-12-0173.1

Fisher, N. I., & Lee, A. J. (1986). Correlation coefficients for random variables on a unit sphere or hypersphere. *Biometrika*, *73*(1), 159–164.

Gerber, H. E. (1985). *Relative-humidity parameterization of the Navy Aerosol Model*

(NAM) (Tech. Rep.). Washington, DC: Naval Research Lab.

Goddijn-Murphy, L., Woolf, D. K., & Callaghan, A. H. (2011). Parameterizations and algorithms for oceanic whitecap coverage. *Journal of Physical Oceanography*, *41*(4), 742-756. doi: 10.1175/2010JPO4533.1

Gong, S. L. (2003). A parameterization of sea-salt aerosol source function for sub- and super-micron particles. *Global Biogeochemical Cycles*, *17*(4). doi: 10.1029/2003GB002079

Grythe, H., Kristiansen, N. I., Groot Zwaaftink, C. D., Eckhardt, S., Ström, J., Tunved, P., … Stohl, A. (2017). A new aerosol wet removal scheme for the Lagrangian particle model FLEXPART v10. *Geoscientific Model Development*, *10*(4), 1447–1466. doi: 10.5194/gmd-10-1447-2017

Grythe, H., Ström, J., Krejci, R., Quinn, P., & Stohl, A. (2014). A review of sea-spray aerosol source functions using a large global set of sea salt aerosol concentration measurements. *Atmospheric Chemistry and Physics*, *14*(3), 1277–1297. doi: 10.5194/acp-14-1277-2014

Hande, L. B., Siems, S. T., & Manton, M. J. (2012). Observed trends in wind speed over the Southern Ocean. *Geophysical Research Letters*, *39*(11). doi: 10.1029/2012GL051734

Henzing, J. S., Olivié, D. J. L., & van Velthoven, P. F. J. (2006). A parameterization of size resolved below cloud scavenging of aerosols by rain. *Atmospheric Chemistry and Physics*, *6*(11), 3363–3375. doi: 10.5194/acp-6-3363-2006

Hertel, O., Christensen, J., Runge, E. H., Asman, W. A., Berkowicz, R., Hovmand, M. F., & Øystein Hov. (1995). Development and testing of a new variable scale air pollution model—ACDEP. *Atmospheric Environment*, *29*(11), 1267–1290. doi: https://doi.org/10.1016/1352-2310(95)00067-9

Hicks, B. B., Baldocchi, D. D., Meyers, T. P., Hosker, R. P., & Matt, D. R. (1987). A preliminary multiple resistance routine for deriving dry deposition velocities from measured quantities. *Water, Air, and Soil Pollution*, *36*(3), 311–330. doi: 10.1007/BF00229675

Hsu, S. A. (1986). A mechanism for the increase of wind stress (drag) coefficient with wind speed over water surfaces: A parametric model. *Journal of Physical Oceanography*, *16*(1), 144-150. doi: 10.1175/1520-0485(1986)016<0144:AMFTIO>2.0.CO;2

Hwang, P. A. (2018). High-wind drag coefficient and whitecap coverage derived from microwave radiometer observations in tropical cyclones. *Journal of Physical Oceanography*, *48*(10), 2221-2232. doi: 10.1175/JPO-D-18-0107.1

Jaeglé, L., Quinn, P. K., Bates, T. S., Alexander, B., & Lin, J.-T. (2011). Global distribution of sea salt aerosols: new constraints from in situ and remote sensing observations. *Atmospheric Chemistry and Physics*, *11*(7), 3137–3157. doi: 10.5194/acp-11-3137-2011

Jia, N., & Zhao, D. (2019, Apr 01). The influence of wind speed and sea states on whitecap coverage. *Journal of Ocean University of China*, *18*(2), 282–292. doi: 10.1007/s11802-019-3808-7

Jiang, H., & Chen, G. (2013). A global view on the swell and wind sea climate by the jason-1 mission: A revisit. *Journal of Atmospheric and Oceanic Technology*, *30*(8), 1833-1841. doi: 10.1175/JTECH-D-12-00180.1

Jolly, B., McDonald, A. J., Coggins, J. H. J., Zawar-Reza, P., Cassano, J., Lazzara, M., … Dale, E. (2016). A validation of the Antarctic mesoscale prediction system using self-organizing maps and high-density observations from SNOWWEB. *Monthly Weather Review*, *144*(9), 3181-3200. doi: 10.1175/MWR-D-15-0447.1

Kaleschke, L., Richter, A., Burrows, J., Afe, O., Heygster, G., Notholt, J., … Jacobi, H.-W. (2004). Frost flowers on sea ice as a source of sea salt and their influence on tropospheric halogen chemistry. *Geophysical Research Letters*, *31*(16). doi: 10.1029/2004GL020655

Kuma, P., McDonald, A. J., Morgenstern, O., Alexander, S. P., Cassano, J. J., Garrett, S., … Williams, J. (2019). Evaluation of Southern Ocean cloud in the HadGEM3 general circulation model and MERRA-2 reanalysis using ship-based observations. *Atmospheric Chemistry and Physics Discussions*, *2019*, 1–37. doi: 10.5194/acp-2019-201

Kyrö, E.-M., Grönholm, T., Vuollekoski, H., Virkkula, A., Kulmala, M., & Laakso, L. (2009). Snow scavenging of ultrafi ne particles: field measurements and parameterization. *Boreal Environment Research*, *14*, 527–538.

Lewis, E., & Schwartz, S. (2004). *Sea salt aerosol production: Mechanisms, methods, measurements and models – a critical review*. Washington, DC: American Geophysical Union.

McCluskey, C. S., Hill, T. C. J., Humphries, R. S., Rauker, A. M., Moreau, S., Strutton, P. G., … DeMott, P. J. (2018). Observations of ice nucleating particles over Southern Ocean waters. *Geophysical Research Letters*, *45*(21), 11,989-11,997. doi: 10.1029/2018GL079981

McCoy, D. T., Burrows, S. M., Wood, R., Grosvenor, D. P., Elliott, S. M., Ma, P.-L., … Hartmann, D. L. (2015). Natural aerosols explain seasonal and spatial patterns of Southern Ocean cloud albedo. *Science Advances*, *1*(6). doi: 10.1126/sciadv.1500157

Modini, R. L., Frossard, A. A., Ahlm, L., Russell, L. M., Corrigan, C. E., Roberts, G. C., … Leaitch, W. R. (2015). Primary marine aerosol-cloud interactions off the coast of California. *Journal of Geophysical Research: Atmospheres*, *120*(9), 4282-4303. doi: 10.1002/2014JD022963

Monahan, E. C. (1971). Oceanic whitecaps. *Journal of Physical Oceanography*, *1*(2), 139-144. doi: 10.1175/1520-0485(1971)001<0139:OW>2.0.CO;2

Monahan, E. C., Spiel, D. E., & Davidson, K. L. (1986). A model of marine aerosol generation via whitecaps and wave disruption. In E. C. Monahan & G. M. Niocaill (Eds.), *Oceanic whitecaps: And their role in air-sea exchange processes* (pp. 167–174). Dordrecht: Springer. doi: 10.1007/978-94-009-4668-2_16

Monahan, E. C., & Ó Muircheartaigh, I. (1980). Optimal power-law description of oceanic whitecap coverage dependence on wind speed. *Journal of Physical Oceanography*, *10*(12), 2094–2099. doi: 10.1175/1520-0485(1980)010<2094:OPLDOO>2.0.CO;2

Murphy, D., Anderson, J., Quinn, P., McInnes, L., Brechtel, F., Kreidenweis, S., … Buseck, P. (1998). Influence of sea-salt on aerosol radiative properties in the Southern Ocean marine boundary layer. *Nature*, *392*, 62–65. doi: 10.1038/32138

Mårtensson, E. M., Nilsson, E. D., de Leeuw, G., Cohen, L. H., & Hansson, H.-C. (2003). Laboratory simulations and parameterization of the primary marine aerosol production. *Journal of Geophysical Research: Atmospheres*, *108*(D9). doi: 10.1029/2002JD002263

Nash, J., & Sutcliffe, J. (1970). River flow forecasting through conceptual models part i — a discussion of principles. *Journal of Hydrology*, *10*(3), 282 - 290. doi: 10.1016/0022-1694(70)90255-6

Norris, S. J., Brooks, I. M., Moat, B. I., Yelland, M. J., de Leeuw, G., Pascal, R. W., & Brooks, B. (2013). Near-surface measurements of sea spray aerosol production over whitecaps in the open ocean. *Ocean Science*, *9*(1), 133–145. Retrieved from `https://www.ocean-sci.net/9/133/2013/` doi: 10.5194/os-9-133-2013

Ortiz-Suslow, D. G., Haus, B. K., Mehta, S., & Laxague, N. J. M. (2016). Sea spray generation in very high winds. *Journal of the Atmospheric Sciences*, *73*(10), 3975–3995. doi: 10.1175/JAS-D-15-0249.1

Ovadnevaite, J., Manders, A., de Leeuw, G., Ceburnis, D., Monahan, C., Partanen, A.-I., … O'Dowd, C. D. (2014). A sea spray aerosol flux parameterization encapsulating wave state. *Atmospheric Chemistry and Physics*, *14*(4), 1837–1852.

doi: 10.5194/acp-14-1837-2014

Petters, M. D., & Kreidenweis, S. M. (2007). A single parameter representation of hygroscopic growth and cloud condensation nucleus activity. *Atmospheric Chemistry and Physics*, *7*(8), 1961–1971. doi: 10.5194/acp-7-1961-2007

Piazzola, J., Forget, P., & Despiau, S. (2002). A sea spray generation function for fetch-limited conditions. *Annales Geophysicae*, *20*(1), 121–131. doi: 10.5194/angeo-20-121-2002

Polar Meteorology Group, Byrd Polar and Climate Research Center. (2018, 7 17). *Antarctic mesoscale prediction system (AMPS) domain 1 forecasts.* data retrieved from Climate Data Gateway at NCAR. Retrieved 17/7/2018, from `https://www.earthsystemgrid.org/project/amps.html`

Popinet, S., Smith, M., & Stevens, C. (2004). Experimental and numerical study of the turbulence characteristics of airflow around a research vessel. *Journal of Atmospheric and Oceanic Technology*, *21*(10), 1575–1589. doi: 10.1175/1520-0426(2004)021<1575:EANSOT>2.0.CO;2

Powell, M. D., Vickery, P. J., & Reinhold, T. A. (2003). Reduced drag coefficient for high wind speeds in tropical cyclones. *Nature*, *422*(6929), 279–283. doi: 10.1038/nature01481

Prather, K. A., Bertram, T. H., Grassian, V. H., Deane, G. B., Stokes, M. D., DeMott, P. J., … Zhao, D. (2013). Bringing the ocean into the laboratory to probe the chemical complexity of sea spray aerosol. *Proceedings of the National Academy of Sciences*, *110*(19), 7550–7555. doi: 10.1073/pnas.1300262110

Quinn, P. K., Coffman, D. J., Johnson, J. E., Upchurch, L. M., & Bates, T. S. (2017). Small fraction of marine cloud condensation nuclei made up of sea spray aerosol. *Nature Geoscience*, *10*, 674–679. doi: 10.1038/ngeo3003

Raphael, M. N., Marshall, G. J., Turner, J., Fogt, R. L., Schneider, D., Dixon, D. A., … Hobbs, W. R. (2016). The Amundsen Sea low: Variability, change, and impact on Antarctic climate. *Bulletin of the American Meteorological Society*, *97*(1), 111-121. doi: 10.1175/BAMS-D-14-00018.1

Revell, L. E., Kremser, S., Hartery, S., Harvey, M., Mulcahy, J. P., Williams, J., … Schuddeboom, A. (2019). The sensitivity of Southern Ocean aerosols and cloud microphysics to sea spray and sulfate aerosol production in the HadGEM3-GA7.1 chemistry-climate model. *Atmospheric Chemistry and Physics Discussions*, *2019*, 1–36. Retrieved from `https://www.atmos-chem-phys-discuss.net/acp-2019-629/` doi: 10.5194/acp-2019-629

Richter, D. H., & Sullivan, P. P. (2013). Sea surface drag and the role of spray. *Geophysical Research Letters*, *40*(3), 656–660. doi: 10.1002/grl.50163

Schuddeboom, A., Varma, V., McDonald, A. J., Morgenstern, O., Harvey, M., Parsons, S., … Furtado, K. (2019). Cluster-based evaluation of model compensating errors: A case study of cloud radiative effect in the Southern Ocean. *Geophysical Research Letters*, *46*(6), 3446-3453. doi: 10.1029/2018GL081686

Schwendeman, M., & Thomson, J. (2015). Observations of whitecap coverage and the relation to wind stress, wave slope, and turbulent dissipation. *Journal of Geophysical Research: Oceans*, *120*(12), 8346-8363. doi: 10.1002/2015JC011196

Sellegri, K., O'Dowd, C. D., Yoon, Y. J., Jennings, S. G., & de Leeuw, G. (2006). Surfactants and submicron sea spray generation. *Journal of Geophysical Research: Atmospheres*, *111*(D22). doi: 10.1029/2005JD006658

Shindell, D. T., Lamarque, J.-F., Schulz, M., Flanner, M., Jiao, C., Chin, M., … Lo, F. (2013). Radiative forcing in the ACCMIP historical and future climate simulations. *Atmospheric Chemistry and Physics*, *13*(6), 2939–2974. doi: 10.5194/acp-13-2939-2013

Slinn, W. (1977). Some approximations for the wet and dry removal of particles and gases from the atmosphere. *Water, Air, and Soil Pollution*, *7*(4), 513–543. doi: 10.1007/BF00285550

Smith, M. J., Ho, D. T., Law, C. S., McGregor, J., Popinet, S., & Schlosser, P. (2011). Uncertainties in gas exchange parameterization during the SAGE dual-tracer experiment. *Deep Sea Research Part II: Topical Studies in Oceanography*, *58*(6), 869 - 881. doi: 10.1016/j.dsr2.2010.10.025

Snyder, R. L., & Kennedy, R. M. (1983). On the formation of whitecaps by a threshold mechanism. part i:. basic formalism. *Journal of Physical Oceanography*, *13*(8), 1482-1492. doi: 10.1175/1520-0485(1983)013<1482:OTFOWB>2.0.CO;2

Stramska, M., & Petelski, T. (2003). Observations of oceanic whitecaps in the north polar waters of the atlantic. *Journal of Geophysical Research: Oceans*, *108*(C3). doi: 10.1029/2002JC001321

Sugihara, Y., Tsumori, H., Ohga, T., Yoshioka, H., & Serizawa, S. (2007). Variation of whitecap coverage with wave-field conditions. *Journal of Marine Systems*, *66*(1), 47 - 60. (5th International Symposium on Gas Transfer at Water Surfaces) doi: https://doi.org/10.1016/j.jmarsys.2006.01.014

Trenberth, K. E., & Fasullo, J. T. (2010). Simulation of present-day and twenty-first-century energy budgets of the Southern Oceans. *Journal of Climate*, *23*(2), 440–454.

Twomey, S. (1977). The influence of pollution on the shortwave albedo of clouds. *Journal of the Atmospheric Sciences*, *34*(7), 1149-1152. doi: 10.1175/1520-0469(1977)034<1149:TIOPOT>2.0.CO;2

Witek, M. L., Diner, D. J., & Garay, M. J. (2016). Satellite assessment of sea spray aerosol productivity: Southern Ocean case study. *Journal of Geophysical Research: Atmospheres*, *121*(2), 872–894. doi: 10.1002/2015JD023726

Xu, D., Liu, X., & Yu, D. (2000). Probability of wave breaking and whitecap coverage in a fetch-limited sea. *Journal of Geophysical Research: Oceans*, *105*(C6), 14253-14259. doi: 10.1029/2000JC900040

Yang, X., Pyle, J. A., & Cox, R. A. (2008). Sea salt aerosol production and bromine release: Role of snow on sea ice. *Geophysical Research Letters*, *35*(16). doi: 10.1029/2008GL034536

Young, I. (1999). Seasonal variability of the global ocean wind and wave climate. *International Journal of Climatology*, *19*(9), 931–950. doi: 10.1002/(SICI)1097-0088(199907)19:9<931::AID-JOC412>3.0.CO;2-O

Young, I. R., Zieger, S., & Babanin, A. V. (2011). Global trends in wind speed and wave height. *Science*, *332*(6028), 451–455. doi: 10.1126/science.1197219

Zábori, J., Krejci, R., Ekman, A. M. L., Mårtensson, E. M., Ström, J., de Leeuw, G., & Nilsson, E. D. (2012). Wintertime Arctic Ocean sea water properties and primary marine aerosol concentrations. *Atmospheric Chemistry and Physics*, *12*(21), 10405–10421. doi: 10.5194/acp-12-10405-2012